Journal of Computational Biophysics and Chemistry

Research

Cite This: *J. Comput. Biophys. Chem.* **2021**, *20* (3), 225–231

Polarizability of Pyruvate Anion in Small Water Clusters

Victor Ruan and Arun K. Sharma*

Department of Chemistry & Physics,
Wagner College, Staten Island, 10301 NY, US

*aksharma@wagner.edu

ABSTRACT: Pyruvate anion is important in a broad array of physicochemical processes ranging from glucose homeostasis to atmospheric reactions. However, the electronic polarizability of the moiety has not been investigated extensively. We present theoretical results from electronic structure calculations on the static and dynamic polarizability of microhydrated pyruvate anions. These investigations were carried out with the $CH_3COCOO^- \cdot n\ H_2O$ clusters ($n = 1$–9) to mimic microhydration conditions. These density functional theory calculations were carried out at the B3LYP/aug-cc-PVTZ level to uncover the optimal geometry of the anion water cluster. Sadlej basis set functions with the B3LYP functional were used to calculate the static and dynamic polarizabilities. Multiple simulated annealing simulations were carried out to discover additional low-lying minima. It is observed that the electronic polarizability varies linearly with the size of the hydrated cluster. Expressions that describe the relationship between the dynamic polarizability and the field frequency are provided for each cluster.

KEYWORDS: Polarizability; microsolvation; clusters; density functional theory.

1. INTRODUCTION

The pyruvate anion, CH_3COCOO^-, aids in the maintenance of glucose homeostasis and ATP production by oxidative phosphorylation.[1–6] Additionally, it also plays a significant role in many chemical atmospheric processes.[7–11] For example, unlike many volatile organic compounds that degrade by hydroxyl radical, pyruvic acid distinctly undergoes direct photolysis that dominates over OH oxidation by several orders of magnitude.[12,13] Due to its carbonyl functional group, pyruvic acid acts as a keto-acid intermediate in isoprene oxidation pathways[14] that provides high acetic acid product yields with a shorter lifetime in the presence of oxygen.[15] Recording accurate descriptions of simple anion–water and water–water interactions within the interfacial region are essential to understand the solvation. Although there are many systematic studies of common inorganic anions like nitrate, bisulfate and bicarbonate,[16–19] there are no systematic studies of pyruvate anion surrounded by a water network.

The study of microhydration of small charged anionic species has recently received widespread attention due to the strong dependence of their properties on the size and geometry of the water network.[20–27] Cluster studies focusing on the structural and electronic properties of hydrated negative ions have shed light on multiple solute–solvent interactions.[28–32] The negatively charged solute in microhydrated systems influences the surrounding water-network geometry in order to accommodate the water–water and water–anion interactions. A detailed understanding of the solvation of ions provides insight into their roles in chemical and biological processes.[33–36] This work focuses on the impact of increasing number of water molecules on the structure and polarizability of the pyruvate anion. We report the fully optimized ground-state structures of $CH_3COCOO^- \cdot n\ H_2O$ clusters ($n = 1$–9). The corresponding anionic polarizability is central in determining ion solvation at both the surface and bulk aerosol. These properties are essential in understanding ion specific behavior at the aerosol interface. Therefore, a study of pyruvate anion in increasing sizes of hydrated clusters is carried out to

Received: 27 May 2020
Accepted: 30 November 2020
Published: 4 January 2021

DOI: 10.1142/S2737416521500095
J. Comput. Biophys. Chem. **2021**, *20* (3), 225–231

examine the static and dynamic polarizability for each cluster. Dynamic polarizability is an important quantity to investigate the distortion of electronic clouds in the molecule when it is exposed to radiation. The dynamic polarizability is required for characterizing various optical properties as well as understanding the intermolecular interactions. The polarizability of a system becomes infinite corresponding to the resonance frequency of the electronic transition for that species. Although there have been some recent efforts on common anions like nitrate,[37–39] there are no detailed investigations on the impact of micro-solvation on the pyruvate anion. This work provides a complete picture of static polarizability and dynamic polarizability for the cluster sizes of $n = 1$–9 water molecules.

2. THEORETICAL METHODS

Hybrid density functional theory calculations with the B3LYP functional and 6-311+G(d, p)[40,41] basis sets were applied for optimized geometry searches for $CH_3COCOO^- \cdot n\ H_2O$ ($n = 1$–9) for all atoms implemented in Gaussian16.[42] The initial geometries were used as starting points for subsequent optimization calculations with Dunning's correlation consistent basis sets at the triple zeta level and augmented with diffuse functions using the keyword aug-cc-pVTZ.[43,44] Geometry optimization calculations were performed to determine the most stable energy minimum structures. This adopted procedure cannot guarantee that the global minimum structure of each respective hydrated cluster was found. Therefore, Monte Carlo[45]-based simulated annealing procedures implemented in TINKER[46] were applied to find other viable local minima. The structures collected from simulated annealing were subjected to further geometry optimization calculations at the same level of theory as previous runs. The optimization results at each stage were checked to ensure that there were no imaginary vibrational frequencies for each structure. The lowest energy structures from the resulting set of structures were putatively labeled as "global minimum" for each cluster and isolated for polarizability calculations. Static and dynamic polarizabilities of the identified global minimum for each cluster were calculated by using time-dependent density functional theory (TD-DFT) method[47–50] and B3LYP functional with the Sadlej[51] set of atomic basis functions. The Sadlej basis set functions were obtained from the Basis Set Exchange.[52] The efficiency and suitability of the Sadlej atomic basis functions has been demonstrated in benchmark studies[53] for the calculation of polarizabilities. The aug-cc-PVTZ basis set and TD-DFT approach have been successfully used in previous comparative studies calculating global minimum structures for microhydrated anion clusters and molecules.[16,49,50,54] Dynamic polarizability was calculated over a field frequency up to 0.16 a.u. The results from these calculations are discussed in the following sections.

3. RESULTS AND DISCUSSION

3.1. Cluster geometry

Full geometry optimization of $CH_3COCOO^- \cdot n\ H_2O$ ($n = 1$–9) was carried out to find the local minimum structure of each respective hydrated cluster. The starting geometry was constructed through chemical intuition. Initial geometry optimization calculations were carried out at the B3LYP/6-311+G(d, p) level of theory. Monte Carlo-based simulated annealing procedures implemented in TINKER[46] were used to find several minimum energy structures. The structures from annealing runs were subjected to optimized geometry calculations with the B3LYP functional and the aug-cc-pVTZ basis sets with DFT calculations to arrive at a collection of structures. The lowest energy structure of each anion–water cluster is provided in Fig. 1. The number of structures considered for each cluster is reported in Table 1. A listing of energy values and structures for the local minima considered in this work are reported in Table S1 and Fig. S1 in the Supporting Information. The effect of hydration is shown by successive addition of water molecules surrounding CH_3COCOO^- species.

A detailed structural analysis of these complexes is beyond the scope of the current investigation. However, there are some general features that can be highlighted. Water molecules surround the anion with hydrogen bonding sites as the oxygen atoms of the carboxyl group and the ketone group. The clusters generally become more spherical in arrangement as the number of water molecules around the anion is increased. This feature has been observed in studies of nitrate anion under similar micro-hydration environment.[55] Some of the minimum energy configurations show surface structure in which the solute resides at the surface of the solvent water network.

3.2. Static and dynamic polarizability

Understanding the response of anionic hydrated clusters to an external electric field is important for

DOI: 10.1142/S2737416521500095
J. Comput. Biophys. Chem. 2021, 20 (3), 225–231

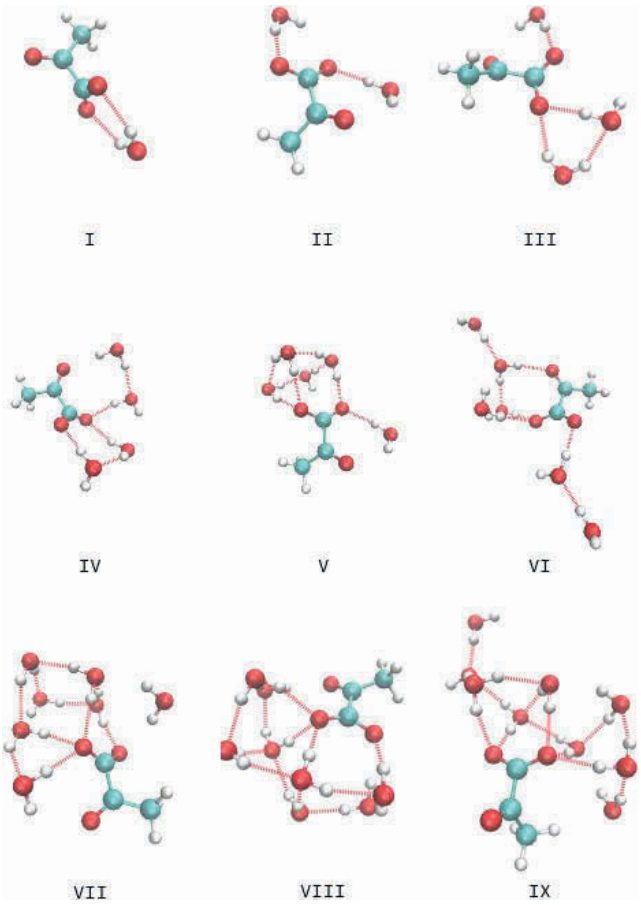

Fig. 1. Optimized minimum structures of each hydrated cluster at DFT/aug-cc-PVTZ level of theory.

analyzing ion solvation. Electronic polarizabilities were calculated for the lowest potential energy structure within each of the anion–water clusters.

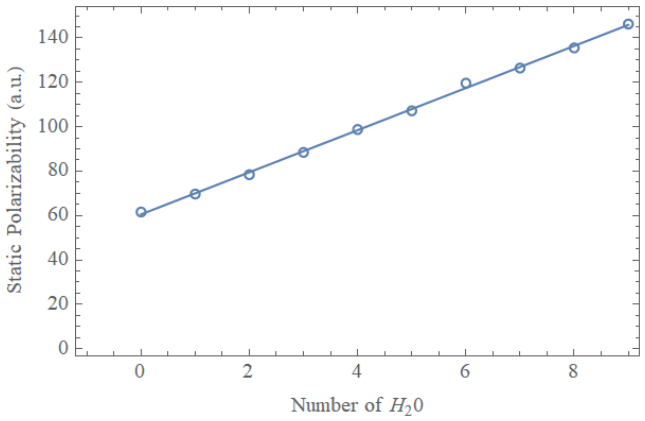

Fig. 2. Variation of static polarizability with respect to cluster size demonstrating the extensive nature of polarizability.

Static and dynamic polarizability at a field frequency of 0.08 a.u. were calculated for the global minimum structures of each respective cluster using TD-DFT[54,56,57] technique employing the Sadlej[51] basis set. The calculated static ($\omega = 0$) and dynamic polarizability ($\omega = 0.08$ a.u.) values for these structures are reported in Table 1. As expected, variation of polarizability relates to the size of the cluster in a linear fashion. The variation of static polarizability with respect to cluster size is displayed in Fig. 2. The best fit equation is $y = 9.49x + 60.6$ with a correlation coefficient of 0.999. The extensive nature of polarizability is highlighted in the linearity of the plot. Dynamic polarizability displays a similar behavior and increases linearly with the increase in the number of water molecules surrounding the anion. The calculated

Table 1. The number of initial structures considered for global geometry optimization is shown in parentheses next to the species. The polarizabilities (a.u.) for H_2O and the most stable structure of $CH_3COCOO^- \cdot n\ H_2O$ ($n = 1$–9) systems are calculated with TD-DFT technique with the Sadlej basis set.

Species	Static polarizability (a.u.)	Dynamic polarizability ($\omega = 0.08$ a.u.)
H_2O	9.98	10.25
CH_3COCOO^-	61.63	66.20
$CH_3COCOO^- \cdot 1H_2O$ (3)	69.73	73.34
$CH_3COCOO^- \cdot 2H_2O$ (3)	78.45	81.98
$CH_3COCOO^- \cdot 3H_2O$ (3)	88.5	92.10
$CH_3COCOO^- \cdot 4H_2O$ (3)	98.81	102.63
$CH_3COCOO^- \cdot 5H_2O$ (3)	107.23	111.03
$CH_3COCOO^- \cdot 6H_2O$ (4)	119.68	123.94
$CH_3COCOO^- \cdot 7H_2O$ (6)	126.49	130.61
$CH_3COCOO^- \cdot 8H_2O$ (8)	135.56	139.85
$CH_3COCOO^- \cdot 9H_2O$ (6)	146.32	150.90

DOI: 10.1142/S2737416521500095
J. Comput. Biophys. Chem. **2021**, *20* (3), 225–231

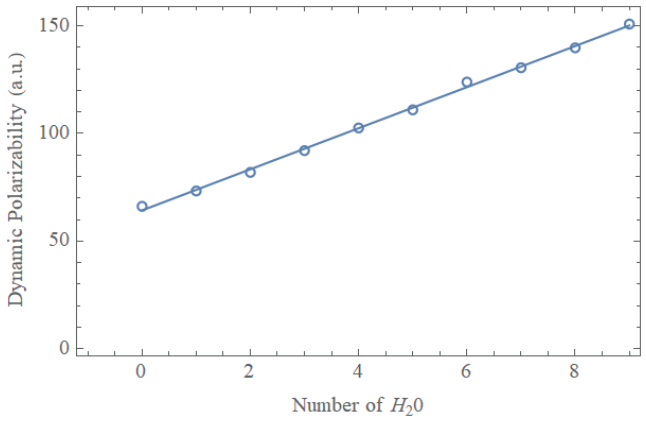

Fig. 3. Variation of dynamic polarizability at half of the maximum field frequency (0.08 a.u) with respect to cluster size demonstrating the extensive nature of polarizability.

dynamic polarizabilities of pyruvate in solvent clusters over an external field frequency ($\omega = 0.08$ a.u.) in steps of 0.01 a.u. is displayed in Fig. 3. The best fit equation is $y = 9.55x + 64.3$ with a correlation coefficient of 0.998.

Numerical equations were fit to the data to analyze the variation in polarizability with the increasing frequency. More specifically, $CH_3COCOO^- \cdot 3H_2O$, $CH_3COCOO^- \cdot 5H_2O$, $CH_3COCOO^- \cdot 7H_2O$, and $CH_3COCOO^- \cdot 9H_2O$ are presented here. The variation of dynamic polarizability can be seen in Fig. 4. The maximum external field frequency is 0.16 a.u. and the polarizability is seen to increase exponentially. Best-fit expressions for the dynamic polarizability have been fit as a function of field frequency. The fit is modeled as static polarizability of the species in combination with an exponential function of the form $\omega = \omega_0 + be^{x/c}$. The best-fit expressions for each cluster are shown in Table 2. All these expressions have a correlation coefficient higher than 0.999. The polarizability increases as a function of increasing field frequency and cluster size. This is in excellent agreement with other studies of microhydrated anions like nitrate.[16,20] The dynamic polarizability for the $CH_3COCOO^- \cdot n\ H_2O$ clusters diverges when the field energy is in the vicinity of 4.36 eV. This indicates that the electronic transition energy is most likely close to 4.36 eV. However, despite extensive literature review, we haven't been able to locate experimental evidence for this transition energy.

3.3. Solute and solvent contribution

The total polarizability of each of the $CH_3COCOO^- \cdot n\ H_2O$ ($n = 1$–9) clusters was partitioned into the contribution of single solute anion and solvent water molecules. The polarizability of CH_3COCOO^- was calculated by removing the surrounding water in the system followed by polarizability calculation. Similarly, the solute pyruvate anion was removed, and the polarizability of the surrounding water molecules was calculated. These calculations were carried out at the same level of theory as previously described and the results are arranged in Table 3. Calculations correspond to half of the maximum field frequency of 0.08 a.u. It is seen that the sum of the calculated polarizability of the free solute and solvent system has an error range from 1.94% to 5.34% with respect to the total

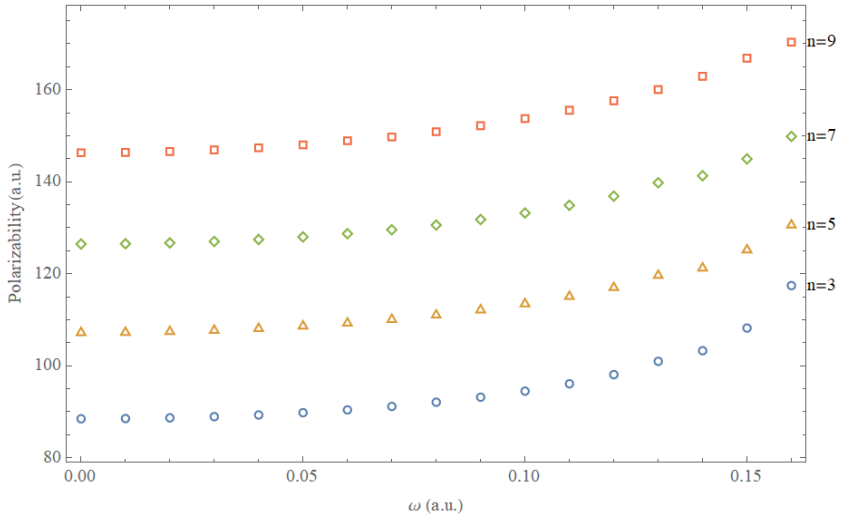

Fig. 4. Variation of dynamic polarizability with external field frequency up to 0.16 a.u. with respect to cluster size.

DOI: 10.1142/S2737416521500095

Table 2. Best-fit equations for dynamic polarizability as a function of field frequency. All the fits have a correlation coefficient higher than 0.999.

Species	Fit equation
CH_3COCOO^-	$\alpha = 62.21 + 0.05\exp(\omega/0.019)$
$CH_3COCOO^- \cdot 1H_2O$	$\alpha = 69.73 + 0.31\exp(\omega/0.034)$
$CH_3COCOO^- \cdot 2H_2O$	$\alpha = 78.45 + 0.32\exp(\omega/0.035)$
$CH_3COCOO^- \cdot 3H_2O$	$\alpha = 88.50 + 0.32\exp(\omega/0.036)$
$CH_3COCOO^- \cdot 4H_2O$	$\alpha = 98.81 + 0.23\exp(\omega/0.033)$
$CH_3COCOO^- \cdot 5H_2O$	$\alpha = 107.23 + 0.47\exp(\omega/0.040)$
$CH_3COCOO^- \cdot 6H_2O$	$\alpha = 119.68 + 0.64\exp(\omega/0.043)$
$CH_3COCOO^- \cdot 7H_2O$	$\alpha = 126.49 + 0.45\exp(\omega/0.039)$
$CH_3COCOO^- \cdot 8H_2O$	$\alpha = 135.56 + 0.69\exp(\omega/0.045)$
$CH_3COCOO^- \cdot 9H_2O$	$\alpha = 146.32 + 0.74\exp(\omega/0.047)$

Table 3. Partitioning of the total polarizability into the contribution of the single solute anion and solvent molecules of the lowest energy structures of $CH_3COCOO^- \cdot n\ H_2O$ ($n = 1$–9) clusters using the Sadlej basis set.

	Static polarizability (a.u.)		Dynamic polarizability ($\omega = 0.08$ a.u.)	
Systems	Solute	Solvent	Solute	Solvent
$CH_3COCOO^- \cdot 1H_2O$	60.03	10.54	63.93	10.83
$CH_3COCOO^- \cdot 2H_2O$	61.24	20.26	65.91	20.83
$CH_3COCOO^- \cdot 3H_2O$	60.74	30.19	65.21	31.01
$CH_3COCOO^- \cdot 4H_2O$	61.06	40.39	65.66	41.52
$CH_3COCOO^- \cdot 5H_2O$	60.73	50.24	65.22	51.62
$CH_3COCOO^- \cdot 6H_2O$	60.99	61.14	65.38	62.86
$CH_3COCOO^- \cdot 7H_2O$	61.00	70.22	65.43	72.15
$CH_3COCOO^- \cdot 8H_2O$	60.18	79.46	64.50	81.62
$CH_3COCOO^- \cdot 9H_2O$	61.26	90.27	65.87	92.79

polarizability. The maximum error is seen with the pyruvate anion cluster with seven water molecules.

4. CONCLUSIONS

The results for the structure and static and dynamic polarizability of $CH_3COCOO^- \cdot n\ H_2O$ clusters ($n = 1$–9) were determined from quantum mechanical calculations. Simulated annealing technique was used to sample geometrical configurations and the lowest energy structures from this investigation were analyzed further. All DFT calculations were carried out with the B3LYP functional and aug-cc-pVTZ basis sets. The polarizability was calculated using the Sadlej basis set functions and the B3LYP functional. It is observed that static and dynamic polarizabilities vary linearly with increasing size of cluster. The partitioning of the single solute anion and solvent molecules was analyzed with respect to the total polarizability. Our expressions fitting polarizability as function of field frequency seem to agree with previous efforts in this domain for different anions. These results serve as an exploration of the polarizability of the microhydrated pyruvate anion. We hope that our calculations will provide an initial point to experimental investigations on this biologically and chemically important species.

AUTHOR CONTRIBUTIONS

This paper was written with the help of all authors contributions. All authors have given approval to the final version of this paper.

ACKNOWLEDGMENTS

This work was supported by the National Science Foundation (Grant No. CHE-1708635). This work used the Extreme Science and Engineering Discovery Environment (XSEDE)[54] resource COMET at San Diego Supercomputer Center through allocation TG-CHE180054.

References

1. Patel, M. S.; Korotchkina, L. G. Regulation of the Pyruvate Dehydrogenase Complex. *Biochem. Soc. Trans.* **2006**, *34* (2), 217–222.
2. McFate, T.; Mohyeldin, A.; Lu, H.; Thakar, J.; Henriques, J.; Halim, N. D.; Wu, H.; Schell, M. J.; Tsz, M. T.; Teahan, O. *et al.* Pyruvate Dehydrogenase Complex Activity Controls Metabolic and Malignant Phenotype in Cancer Cells. *J. Biol. Chem.* **2008**, *283* (33), 22700–22708.
3. Gray, L. R.; Tompkins, S. C.; Taylor, E. B. Regulation of Pyruvate Metabolism and Human Disease. *Cell. Mol. Life Sci.* **2014**, *71* (14), 2577–2604.
4. Christofk, H. R.; Vander Heiden, M. G.; Harris, M. H.; Ramanathan, A.; Gerszten, R. E.; Wei, R.; Fleming, M. D.; Schreiber, S. L.; Cantley, L. C. The M2 Splice Isoform of Pyruvate Kinase Is Important for Cancer Metabolism and Tumour Growth. *Nature* **2008**, *452* (7184), 230–233.
5. Desagher, S.; Glowinski, J. Pyruvate Protects Neurons against Hydrogen. *J. Neurosci.* **1997**, *17* (23), 9060–9067.
6. Steensmays, H. Y.; Pronk, J.; Dijken, V. J. Pyruvate Metabolism in Saccharomyces Cerevisiae. *Yeast* **1996**, *12*, 1607–1633.
7. Andreae, M. O.; Talbot, R. W.; Li, S. M. Atmospheric Measurements of Pyruvic and Formic Acid. *J. Geophys. Res.* **1987**, *92* (D6), 6635–6641.
8. Boris, A. J.; Desyaterik, Y.; Collett, J. L. How Do Components of Real Cloud Water Affect Aqueous Pyruvate Oxidation? *Atmos. Res.* **2014**, *143*, 95–106.

9. Griffith, E. C.; Carpenter, B. K.; Shoemaker, R. K.; Vaida, V. Photochemistry of Aqueous Pyruvic Acid. *Proc. Natl. Acad. Sci. U. S. A.* **2013**, *110* (29), 11714–11719.
10. Reed Harris, A. E.; Pajunoja, A.; Cazaunau, M.; Gratien, A.; Pangui, E.; Monod, A.; Griffith, E. C.; Virtanen, A.; Doussin, J. F.; Vaida, V. Multiphase Photochemistry of Pyruvic Acid under Atmospheric Conditions. *J. Phys. Chem. A* **2017**, *121* (18), 3327–3339.
11. Yang, H.; Wang, N.; Pang, S. F.; Zheng, C. M.; Zhang, Y. H. Chemical Reaction between Sodium Pyruvate and Ammonium Sulfate in Aerosol Particles and Resultant Sodium Sulfate Efflorescence. *Chemosphere* **2019**, *215*, 554–562.
12. Mellouki, A.; Mu, Y. On the Atmospheric Degradation of Pyruvic Acid in the Gas Phase. **2003**, *157*, 295–300.
13. Epstein, S. A.; Nizkorodov, S. A. A Comparison of the Chemical Sinks of Atmospheric Organics in the Gas and Aqueous Phase. *Atmos. Chem. Phys. Discuss.* **2012**, *12* (4), 10015–10058.
14. Carlton, A. G.; Turpin, B. J.; Lim, H. J.; Altieri, K. E.; Seitzinger, S. Link between Isoprene and Secondary Organic Aerosol (SOA): Pyruvic Acid Oxidation Yields Low Volatility Organic Acids in Clouds. *Geophys. Res. Lett.* **2006**, *33* (6), 2–5.
15. Reed Harris, A. E.; Cazaunau, M.; Gratien, A.; Pangui, E.; Doussin, J. F.; Vaida, V. Atmospheric Simulation Chamber Studies of the Gas-Phase Photolysis of Pyruvic Acid. *J. Phys. Chem. A* **2017**, *121* (44), 8348–8358.
16. Pathak, A. K. Theoretical Study on Microhydration of NO3- Ion: Structure and Polarizability. *Chem. Phys.* **2011**, *384* (1–3), 52–56.
17. Garand, E.; Wende, T.; Goebbert, D. J.; Bergmann, R.; Meijer, G.; Neumark, D. M.; Asmis, K. R. Infrared Spectroscopy of Hydrated Bicarbonate Anion Clusters: HCO 3-(H_2O)1-10. *J. Am. Chem. Soc.* **2010**, *132* (2), 849–856.
18. Yacovitch, T. I.; Wende, T.; Jiang, L.; Heine, N.; Meijer, G.; Neumark, D. M.; Asmis, K. R. Infrared Spectroscopy of Hydrated Bisulfate Anion Clusters: HSO 4-(H_2O)1-16. *J. Phys. Chem. Lett.* **2011**, *2* (17), 2135–2140.
19. Wang, X. Bin; Yang, X.; Wang, L. S.; Nicholas, J. B. Photodetachment and Theoretical Study of Free and Water-Solvated Nitrate Anions, NO3-(H_2O)n (N = 0-6). *J. Chem. Phys.* **2002**, *116* (2), 561–570.
20. Pathak, A. K.; Mukherjee, T.; Maity, D. K. Microhydration of NO3-: A Theoretical Study on Structure, Stability and IR Spectra. *J. Phys. Chem. A* **2008**, *112* (15), 3399–3408.
21. Ali, S. M.; De, S.; Maity, D. K. Microhydration of Cs+ Ion: A Density Functional Theory Study on Cs+-(H_2O)n Clusters (N = 1-10). *J. Chem. Phys.* **2007**, *127* (4), 1–12.
22. Price, E. A.; Hammer, N. I.; Johnson, M. A. A Cluster Study of Cl 2- Microhydration: Size-Dependent Competition between Symmetrical H-Bonding to the Anion and the Formation of Cyclic Water Networks in the Cl 2- · 1- 5(H 2O) Series. *J. Phys. Chem. A* **2004**, *108* (18), 3910–3915.
23. Jungwirth, P.; B. J. F.-P.; Tobias, D. J. Introduction: Structure and Chemistry at Aqueous Interfaces. *Chem. Rev.* **2006**, *106* (4), 1137–1139.
24. Cabarcos, O. M.; Weinheimer, C. J.; Lisy, J. M.; Xantheas, S. S. Microscopic Hydration of the Fluoride Anion. *J. Chem. Phys.* **1999**, *110* (1), 5–8.
25. Ayala, R.; Martínez, J. M.; Pappalardo, R. R.; Saint-Martin, H.; Ortega-Blake, I.; Marcos, E. S. Development of First-Principles Interaction Model Potentials. An Application to the Study of the Bromide Hydration. *J. Chem. Phys.* **2002**, *117* (23), 10512–10524.
26. Marcum, J. C.; Weber, J. M. Microhydration of Nitromethane Anions from Both a Solute and Solvent Perspective. *J. Phys. Chem. A* **2010**, *114* (34), 8933–8938.
27. Mondal, S.; Teja, A. U.; Singh, P. C. Theoretical Study on the Microhydration of Atmospherically Important Carbonyl Sulfide in Its Neutral and Anionic Forms: Bridging the Gap between the Bulk and Finite Size Microhydrated Cluster. *J. Phys. Chem. A* **2015**, *119* (15), 3644–3652.
28. Peng, C.; Chan, C. K. The Water Cycles of Water-Soluble Organic Salts of Atmospheric Importance. *Atmos. Environ.* **2001**, *35* (7), 1183–1192.
29. Robertson, W. H.; Johnson, M. A. Molecular Aspects of Halide Ion Hydration: The Cluster Approach. *Annu. Rev. Phys. Chem.* **2003**, *54* (1), 173–213.
30. Deka, A.; Deka, R. C. Structural and Electronic Properties of Stable Aun (n = 2-13) Clusters: A Density Functional Study. *J. Mol. Struct. Theochem* **2008**, *870* (1–3), 83–93.
31. Castro, M.; Liu, S. R.; Zhai, H. J.; Wang, L. S. Structural and Electronic Properties of Small Titanium Clusters: A Density Functional Theory and Anion Photoelectron Spectroscopy Study. *J. Chem. Phys.* **2003**, *118* (5), 2116–2123.
32. Wan, Q.; Spanu, L.; Galli, G. Solvation Properties of Microhydrated Sulfate Anion Clusters: Insights from Ab Initio Calculations. *J. Phys. Chem. B* **2012**, *116* (31), 9460–9466.
33. Bajaj, P.; Riera, M.; Lin, J. K.; Mendoza Montijo, Y. E.; Gazca, J.; Paesani, F. Halide Ion Microhydration: Structure, Energetics, and Spectroscopy of Small Halide-Water Clusters. *J. Phys. Chem. A* **2019**, *123* (13), 2843–2852.
34. Jee, J. E.; Pestovsky, O.; Bakac, A. Preparation and Characterization of Manganese(IV) in Aqueous Acetic Acid. *Dalt. Trans.* **2010**, *39* (48), 11636–11642.
35. Flórez, E.; Acelas, N.; Ibargüen, C.; Mondal, S.; Cabellos, J. L.; Merino, G.; Restrepo, A. Microsolvation of NO_3^-: Structural Exploration and Bonding Analysis. *RSC Adv.* **2016**, *6* (76), 71913–71923.
36. Wick, C. D.; Dang, L. X. Recent Advances in Understanding Transfer Ions across Aqueous Interfaces. *Chem. Phys. Lett.* **2008**, *458* (1–3), 1–5.

37. Tongraar, A.; Tangkawanwanit, P.; Rode, B. M. A Combined QM/MM Molecular Dynamics Simulations Study of Nitrate Anion (NO 3 -) in Aqueous Solution. *J. Phys. Chem. A* **2006**, *110* (47), 12918–12926.
38. Zhao, L.; Tao, L.; Lin, S. Molecular Dynamics Characterizations of the Supercritical CO2-Mediated Hexane-Brine Interface. *Ind. Eng. Chem. Res.* **2015**, *54* (9), 2489–2496.
39. Waterland, M. R.; Stockwell, D.; Kelley, A. M. Symmetry Breaking Effects in NO3-: Raman Spectra of Nitrate Salts and Ab Initio Resonance Raman Spectra of Nitrate-Water Complexes. *J. Chem. Phys.* **2001**, *114* (14), 6249–6258.
40. Wiberg, K. B. Basis Set Effects on Calculated Geometries: 6-311++G** vs. Aug-Cc-PVDZ. *J. Comput. Chem.* **2004**, *25* (11), 1342–1346.
41. Hertwig, R. H.; Koch, W. On the Parameterization of the Local Correlation Functional. What Is Becke-3-LYP? *Chem. Phys. Lett.* **1997**, *268* (5–6), 345–351.
42. Frisch, M. J.; Trucks, G. W.; Schlegel, H. B.; Scuseria, G. E.; Robb, M. A.; Cheeseman, J. R.; Scalmani, G.; Barone, V.; Petersson, G. A.; Nakatsuji, H.; *et al.* Gaussian16 Revision A.03. 2016.
43. Goldey, M.; Dutoi, A.; Head-Gordon, M. Attenuated Second-Order Møller-Plesset Perturbation Theory: Performance within the Aug-Cc-PVTZ Basis. *Phys. Chem. Chem. Phys.* **2013**, *15* (38), 15869–15875.
44. Hashimoto, T.; Hirao, K.; Tatewaki, H. Comment on Dunning's Correlation-Consistent Basis Sets. *Chem. Phys. Lett.* **1995**, *243* (1–2), 190–192.
45. Metropolis, N.; Ulam, S. The Monte Carlo Method. *J. Am. Stat. Assoc.* **1949**, *44* (247), 335–341.
46. Lagardère, L.; Jolly, L. H.; Lipparini, F.; Aviat, F.; Stamm, B.; Jing, Z. F.; Harger, M.; Torabifard, H.; Cisneros, G. A.; Schnieders, M. J.; *et al.*. Tinker-HP: A Massively Parallel Molecular Dynamics Package for Multiscale Simulations of Large Complex Systems with Advanced Point Dipole Polarizable Force Fields. *Chem. Sci.* **2018**, *9* (4), 956–972.
47. Feng, X. J.; Cao, T. T.; Zhao, L. X.; Lei, Y. M.; Luo, Y. Structural and Electronic Properties of Ren ($n = 8$) Clusters by Density-Functional Theory. *Eur. Phys. J. D* **2008**, *50* (3), 285–288.
48. Kendall, R. A.; Dunning, T. H.; Harrison, R. J.; Kendall, R. A.; Dunning, T. H.; Harrison, R. J. Electron Affinities of the Firstrow Atoms Revisited. Systematic Basis Sets and Wave Functions and Wave Functions. *J. Chem. Phys.* **1992**, *96*, 6796.
49. Campo-Cacharrõn, A.; Cabaleiro-Lago, E. M.; Rodríguez-Otero, J. A DFT Study of the Interaction between Microhydrated Anions and Naphthalendiimides. *Chem. Phys. Chem.* **2012**, *13* (2), 570–577.
50. Sudolská, M.; Cantrel, L.; Černušák, I. Microhydration of Caesium Compounds: Cs, CsOH, CsI and Cs2I 2 Complexes with One to Three H_2O Molecules of Nuclear Safety Interest. *J. Mol. Model.* **2014**, *20* (4), 2218.
51. Sadlej, A. J. Medium-Size Polarized Basis Sets for High-Level Correlated Calculations of Molecular Electric Properties. *Collect. Czechoslov. Chem. Commun.* **1988**, *53* (9), 1995–2016.
52. Pritchard, B. P.; Altarawy, D.; Didier, B.; Gibson, T. D.; Windus, T. L. New Basis Set Exchange: An Open, Up-to-Date Resource for the Molecular Sciences Community. *J. Chem. Inf. Model.* **2019**, *59* (11), 4814–4820.
53. Hammond, J. R.; Govind, N.; Kowalski, K.; Autschbach, J.; Xantheas, S. S. Accurate Dipole Polarizabilities for Water Clusters $N = 2$-12 at the Coupled-Cluster Level of Theory and Benchmarking of Various Density Functionals. *J. Chem. Phys.* **2009**, *131* (21), 1–9.
54. Lange, A.; Herbert, J. M. Simple Methods to Reduce Charge-Transfer Contamination in Time-Dependent Density-Functional Calculations of Clusters and Liquids. *J. Chem. Theory Comput.* **2007**, *3* (5), 1680–1690.
55. Pathak, A. K.; Mukherjee, T.; Maity, D. K. Microhydration of NO 3-: A Theoretical Study on Structure, Stability and IR Spectra. *J. Phys. Chem. A* **2008**, *112* (15), 3399–3408.
56. Marques, M. A. L.; Castro, A.; Rubio, A. Assessment of Exchange-Correlation Functionals for the Calculation of Dynamical Properties of Small Clusters in Time-Dependent Density Functional Theory. *J. Chem. Phys.* **2001**, *115* (7), 3006–3014.
57. Stener, M.; Decleva, P. Time-Dependent Density Functional Calculations of Molecular Photoionization Cross Sections: N2 and PH3. *J. Chem. Phys.* **2000**, *112* (24), 10871–10879.

DOI: 10.1142/S2737416521500095
J. Comput. Biophys. Chem. **2021**, *20* (3), 225–231